



1 **Recent decrease trend of atmospheric mercury concentrations in East China: the**  
2 **influence of anthropogenic emissions**

3 Yi Tang<sup>1,2</sup>, Shuxiao Wang<sup>1,2\*</sup>, Qingru Wu<sup>1,2\*</sup>, Kaiyun Liu<sup>1,2</sup>, Long Wang<sup>3</sup>, Shu Li<sup>1</sup>, Wei Gao<sup>4</sup>, Lei  
4 Zhang<sup>5</sup>, Haotian Zheng<sup>1,2</sup>, Zhijian Li<sup>1</sup>, Jiming Hao<sup>1,2</sup>

5

6 <sup>1</sup> State Key Joint Laboratory of Environmental Simulation and Pollution Control, School of  
7 Environment, Tsinghua University, Beijing 100084, China

8 <sup>2</sup> State Environmental Protection Key Laboratory of Sources and Control of Air Pollution Complex,  
9 Beijing 100084, China

10 <sup>3</sup> School of Environment and Energy, South China University of Technology, Guangzhou, 510006,  
11 China

12 <sup>4</sup> Yangtze River Delta Center for Environmental Meteorology Prediction and Warning, Shanghai,  
13 20030, China

14 <sup>5</sup> State Key Laboratory of Pollution Control & Resource Reuse, School of the Environment, Nanjing  
15 University, Nanjing, 210023, China

16

17

18 \* Correspondence to: Shuxiao Wang (shxwang@tsinghua.edu.cn)

19 Qingru Wu (wuqingru06@163.com)

20

21 **Abstract**

22 Measurements of gaseous elemental Hg (GEM), other air pollutants including SO<sub>2</sub>, NO<sub>x</sub>, O<sub>3</sub>,  
23 PM<sub>2.5</sub>, CO, and meteorological conditions were carried out at Chongming Island in East China from  
24 March 1 in 2014 to December 31 in 2016. During the sampling period, GEM concentrations  
25 significantly decreased from 2.68±1.07 ng m<sup>-3</sup> in 2014 to 1.60±0.56 ng m<sup>-3</sup> in 2016. Monthly mean  
26 GEM concentrations showed a significant decrease with a rate of -0.60 ng m<sup>-3</sup> yr<sup>-1</sup> (R<sup>2</sup>=0.6389,  
27 p<0.01 significance level). Combining the analysis of potential source contribution function (PSCF),  
28 principle component analysis (PCA), and emission inventory, we found that Yangtze River Delta  
29 (YRD) region was the dominant source region of atmospheric mercury in Chongming Island and



30 the main source industries included coal-fired power plants, coal-fired industrial boilers, and cement  
31 clinker production. We further quantified the effect of emission change on the air Hg concentration  
32 variations at Chongming Island through a coupled method of trajectory clusters and air Hg  
33 concentrations. It was find that the reduction of domestic emissions was the main driver of GEM  
34 decline in Chongming Island, accounting for 66% of the total decline. The results indicated that air  
35 pollution control policies targeting SO<sub>2</sub>, NO<sub>x</sub> and particulate matter reductions had significant co-  
36 benefits on atmospheric mercury.



## 37 **1 Introduction**

38 Mercury (Hg) is of crucial concern to public health and the global environment for its  
39 neurotoxicity, long-distance transport, and bioaccumulation. The atmosphere is an important  
40 channel for global mercury transport. Once atmospheric Hg deposits to the aquatic system, it can be  
41 transformed into methylmercury (MeHg) which bio-accumulates through the food web and affects  
42 the central nervous system of human beings (Mason et al., 1995). Hg is therefore on the priority list  
43 of several international agreements and conventions dealing with environmental protection,  
44 including the *Minamata Convention on Mercury*.

45 Atmospheric Hg exists in three operationally defined forms: gaseous elemental mercury (GEM),  
46 gaseous oxidized mercury (GOM), and particulate-bound mercury (PBM). And the sum of GEM  
47 and GOM is known as total gaseous mercury (TGM). In the atmosphere, Hg mainly presents as  
48 GEM, accounting for over 95% of the total. GEM is stable in the troposphere with a long residence  
49 time (0.5 - 2 years) and can be transported at regional and global scale (Lindberg et al., 2007). GEM  
50 can be oxidized through photochemical reaction to GOM, which can be converted to PBM upon  
51 adsorption/absorption on aerosol surfaces. Both GOM and PBM are more soluble and quickly  
52 scavenged through dry and wet deposition (Schroeder and Munthe, 1998).

53 The atmospheric Hg observation results are important evidences to assess the effect of Hg  
54 emission control. During the past decades, significant decreases of GEM concentrations in Europe  
55 and North America have been observed (Cole et al., 2013; Weigelt et al., 2015). Air Hg  
56 concentrations in the northern hemisphere are reported to decline by 30-40% between 1990 and  
57 2010 (Zhang Y et al., 2016). Such a decrease is consistent with the decrease in anthropogenic Hg  
58 emissions inventory in Europe and North America (Streets et al., 2011). So far, most of the long-  
59 term observations on the ground sites have been carried out in the developed countries. For the  
60 developing countries such as China, limited atmospheric Hg observations have been carried out (Fu  
61 et al., 2008b; Zhang H et al., 2016; Hong et al., 2016) and there is no official national monitoring  
62 network of atmospheric Hg. Therefore, there are few continuous multi-year observation records of  
63 China's air Hg published (Fu et al., 2015).

64 China is the largest emitter of atmospheric Hg in the world. Atmospheric Hg emissions in China



65 accounted for 27% of the global total in 2010 (UNEP, 2013), which led to high air Hg concentrations  
66 in China. Therefore, atmospheric Hg observations in China are critical to understand the Hg cycling  
67 at both regional and global scale. China's Mercury emissions had increased from 147 t yr<sup>-1</sup> in 1978  
68 to around 538 t yr<sup>-1</sup> in 2010 due to the dramatic economic development (Zhang L et al., 2015; Wu  
69 et al., 2016; Hui et al., 2017). Atmospheric mercury monitoring that spanned the longest periods  
70 (from 2002 to 2010) in Guiyang, southwestern China witnessed the increase of mercury emissions  
71 in China (Fu et al., 2011). However, recently atmospheric Hg emissions in China have been  
72 estimated decreasing since 2012 (Wu et al., 2016). This decreasing trend needs to be confirmed by  
73 atmospheric Hg observations.

74 In this study, we measured GEM, other air pollutants (eg., PM<sub>2.5</sub> and NO<sub>x</sub>), and meteorological  
75 parameters (eg., temperature and wind speed) at a remote marine site of Chongming Island in East  
76 China during 2014-2016. We analyzed annual and seasonal variation of GEM and the potential  
77 impact factors. Combining the analysis of potential source contribution function (PSCF), principle  
78 component analysis (PCA), and emission inventory, the potential source regions and source  
79 industries of atmospheric Hg pollution at the monitoring site are identified. In addition, a coupled  
80 trajectories and air Hg concentration method is developed to assess the effect of Hg emission change  
81 from different regions on air GEM concentration variation at the monitoring site.

## 82 **2 Materials and methods**

### 83 **2.1 Site descriptions**

84 The monitoring remote site (31°32'13"N, 121°58'04"E, about 10 m above sea level) locates at the  
85 top of weather station in Dongtan Birds National Natural Reserve, Chongming Island, China (Figure  
86 1). As China's third largest island, Chongming Island locates in the east of Yangtze River Delta  
87 region with a typical subtropical monsoon climate. It is rainy, hot, with southern and southeastern  
88 winds in summer and is dry, cold, and with northwestern wind in winter. The dominant surface types  
89 are farmland and wetland. There are no large anthropogenic emission sources in the island and no  
90 habitants within 5 km distance from the site. The downtown Shanghai area is 50 km to the southwest  
91 of the site.



## 92 2.2 Sampling methods and analysis

93 During the monitoring period, we used Tekran™ 2537X/1130/1135 instruments to monitor  
94 speciated Hg in the atmosphere, which was widely used for air Hg observation in the world.  
95 Continuous 5-minute of GEM was measured by Tekran™ 2537X Hg vapor analyzer with the  
96 detection limit of  $0.1 \text{ ng m}^{-3}$  at a sampling flow rate of  $1.0 \text{ L min}^{-1}$  during two campaigns: March  
97 1, 2014 to December 31, 2015 and March 26 to December 31, 2016. The sampling inlet was 1.5 m  
98 above the instrument platform.

99 The 2537X analyzer was calibrated automatically every 25 h using the internal Hg permeation  
100 source inside the instrument, and the internal permeation source was calibrated every 12 months  
101 with manual injection of Hg by a syringe from an external Hg source (module 2505). Two zero and  
102 two span calibrations were performed for each calibration of gold trap A and B, respectively. The  
103 error between gold trap A and gold trap B was limited to  $\pm 10 \%$ . The impactor plates and quartz  
104 filter were changed in every two weeks. The quartz filter was changed once a month. The denuders  
105 were recoated once every two weeks following the procedure developed by Landis et al. (2002).

106 During the sampling campaigns,  $\text{PM}_{2.5}$ ,  $\text{O}_3$ ,  $\text{NO}_x$ , CO and  $\text{SO}_2$  were also monitored by Thermo  
107 Scientific TEOM 1405D, Model 49i  $\text{O}_3$  Analyzer, Model 48i CO Analyzer, Model 42i-TL  $\text{NO}_x$   
108 Analyzer and Model 43i  $\text{SO}_2$  Analyzer, respectively. The detection limits of  $\text{O}_3$ ,  $\text{SO}_2$ ,  $\text{NO}_x$ , CO and  
109  $\text{PM}_{2.5}$  are 1.0, 0.5, 0.4, 0.04 and  $0.1 \text{ } \mu\text{g m}^{-3}$ , respectively. The meteorological parameters including  
110 air temperature, wind speed, and wind direction are measured by Vantage Pro2 weather station  
111 (Davis Instruments). The instruments are tested and calibrated periodically. All data are hourly  
112 averaged in this study.

## 113 2.3 Sources apportionment of atmospheric mercury pollution

### 114 2.3.1 PSCF model

115 To identify the source areas for pollutants with a relatively long lifetime such as GEM (Xu and  
116 Akhtar, 2010), the PSCF values for mean GEM concentrations in grid cells in a study domain are  
117 calculated by counting the trajectory segment endpoints that terminate within each cell. The number  
118 of endpoints that fall in the  $ij$ -th cell are designated  $n_{ij}$ . The number of endpoints for the same cell  
119 having arrival times at the monitoring site corresponding to GEM concentrations higher than a  
120 specific criterion is defined to be  $m_{ij}$ . The criterion in this study is set as the average Hg concentration



121 during our study period. The PSCF value for the  $ij$ -th cell is then defined as:

$$122 \quad PSCF_{ij} = \frac{m_{ij}}{n_{ij}} W_{ij} \quad (1)$$

123 where  $W_{ij}$  is an empirical weight to reduce the effects of grid cells with small  $n_{ij}$  values. In this  
124 study,  $W_{ij}$  is defined as in the following formula, in which  $Avg$  is the mean  $n_{ij}$  of all grid cells with  
125  $n_{ij}$  greater than zero:

$$126 \quad W_{ij} = \begin{cases} 1.0 & n_{ij} > 2 * Avg \\ 0.7 & Avg < n_{ij} \leq 2 * Avg \\ 0.42 & 0.5 * Avg < n_{ij} \leq Avg \\ 0.17 & n_{ij} \leq 0.5 * Avg \end{cases} \quad (2)$$

127 The PSCF value indicates the probability of a grid cell through which polluted events occurs.  
128 More method details can be found in the study of Polissar et al. (Polissar et al., 1999). In this study,  
129 the domain that covered the potential contribution source region ( $105^{\circ}$ – $135^{\circ}$  E,  $15^{\circ}$ – $45^{\circ}$  N) was  
130 divided into 22500 grid cells with  $0.2^{\circ} \times 0.2^{\circ}$  resolution. 72-hour back trajectories were generated  
131 hourly from 1 March, 2014 to 31 December, 2015 and from March 26 to December 31 in 2016 by  
132 TrajStat, a software including HYSPLIT for trajectory calculation with trajectory statistics modules  
133 (Wang et al., 2009). PSCF map was plotted using ArcGIS version 10.1.

#### 134 2.3.2 Principal component analysis (PCA)

135 Correlation between Hg and other pollutant concentrations are used to identify source industries.  
136 Strong positive loadings (loading>0.40) with SO<sub>2</sub> and PM<sub>2.5</sub> typically indicate the impact of coal  
137 combustion, and strong positive loadings with GEM and CO have often been used as an indicator  
138 for regional transport because both pollutants have similar source and stable chemical properties  
139 (Lin et al., 2006; Pirrone et al., 1996). In this study, PCA was applied to infer the possible influencing  
140 factors of GEM in 2014 and 2016. Prior to analysis, each variable was normalized by dividing its  
141 mean, and pollutant concentrations (SO<sub>2</sub>, CO, NO<sub>x</sub>, PM<sub>2.5</sub>) were averaged to 1-h sampling intervals  
142 to match the hourly mercury monitoring during sampling period. The results in 2016 had no CO  
143 data due to instrument broken. Statistics analyses were carried out by using SPSS 19.0 software.

#### 144 2.4 Quantification method of source contribution

145 To further quantitatively assess the effect of change in emissions from different regions on air  
146 concentrations variation at a certain monitoring site, a quantitative estimation method which coupled  
147 trajectories with air Hg concentrations was developed. We firstly identified the trajectories by using



148 the National Oceanic and Atmospheric Administration (NOAA) Hybrid Single-Particle Lagrangian  
 149 Integrated Trajectory (HYSPPLIT) model. The gridded meteorological data at a horizontal resolution  
 150 of  $1^\circ \times 1^\circ$  were obtained from the Global Data Assimilation System (GDAS) (Draxler and Hess,  
 151 1998). The starting heights were set to be 500 m above ground level to represent the center height  
 152 of boundary layer where pollutants are usually well mixed in boundary layer. Secondly, each  
 153 trajectory was assigned with GEM concentration by matching the arriving time in Chongming site.  
 154 Third, the backward trajectories which coupled with Hg concentrations were clustered into groups  
 155 according to transport patterns by using NOAA HYSPPLIT 4.7. Thus, the grouped clusters were  
 156 applied to identify the Hg source regions. The Hg average concentration of the cluster  $j$  was then  
 157 calculated as equation (3). And, the trajectory weighted concentration in the cluster  $j$  as equation  
 158 (4). At last, the contribution of reduction at a certain region on Hg concentration at monitoring sites  
 159 in a certain period can be calculated as equation (5).

160

$$161 \quad C_{j,t} = \frac{\sum_{i=1}^n C_{i,j,t}}{\sum_{i=1}^n N_{i,j,t}} \quad (3)$$

$$162 \quad TWC_{j,t} = \frac{\sum_{i=1}^n N_{i,j,t}}{\sum_{j=1}^m \sum_{i=1}^n N_{i,j,t}} \times C_{j,t} \quad (4)$$

163

164 where  $N$  refers to a certain trajectory.  $j$  refers to a certain cluster.  $t$  is the studied period, and  $n$  is  
 165 the number of trajectory.  $m$  is the number of cluster.  $C$  is the GEM concentration,  $\text{ng m}^{-3}$ .  $TWC$  refers  
 166 to the trajectory weighted concentration,  $\text{ng m}^{-3}$

$$167 \quad CR_j = \frac{TWC_{j,t_2} - TWC_{j,t_1}}{\sum_{j=1}^m TWC_{j,t_2} - \sum_{j=1}^m TWC_{j,t_1}} \quad (5)$$

168 where  $CR$  refers to the contribution of GEM reduction.  $t_1$  and  $t_2$  refers to the two period  
 169 participating to comparison, namely year 2014 and 2016 in this study, respectively.

170 This approach is a simple method to quantify the influence of anthropogenic emissions on GEM



171 concentration variation. It should be noted that errors always exist in calculating trajectories, causing  
172 uncertainties in all trajectory-based approaches. Trajectory errors vary considerably in different  
173 situation. Draxler (1996) suggested uncertainties might be 10% of the travel distance. Besides, this  
174 method required similar meteorological conditions of the periods participated in comparison so as  
175 to reduce the interference from meteorology.

## 176 **2.5 Regional atmospheric Hg emissions**

177 Regional atmospheric Hg emissions by month are calculated by using both the technology-based  
178 emission factor methods and transformed normal distribution function method. Detailed  
179 introduction of these two methods are described in our previous study (Wu et al., 2016).  
180 Conventional air pollutant (SO<sub>2</sub>, PM<sub>2.5</sub>, and NO<sub>x</sub>) emissions were calculated following the study of  
181 Zhao et al. (2013). The source regions included in the emission inventory consisted of Shanghai,  
182 Jiangsu, Zhejiang, and Anhui provinces according to the PSCF results (See section 3.3). The studied  
183 emission sectors included coal-fired power plants, coal-fired industrial boilers, residential coal-  
184 combustion, cement clinker production, iron and steel production, zinc smelting, lead smelting and  
185 other small emission sectors (eg., municipal solid incineration, biomass incineration, copper  
186 smelting, aluminum production, gold production, other coal combustion, oil combustion, and  
187 cremation). The monthly Hg emissions were mainly distributed according to fuel combustions or  
188 products productions by month (Table S1). For small emission sectors, the annual emissions were  
189 equally distributed into monthly emissions. The GEM emissions from natural sources followed the  
190 study of Wang et al. (2016).

## 191 **3 Results and discussions**

### 192 **3.1 Decreasing trends of atmospheric Hg during 2014-2016**

193 The average concentrations of GEM in 2014 and 2016 were  $2.68 \pm 1.07 \text{ ng m}^{-3}$  and  $1.60 \pm 0.56 \text{ ng}$   
194  $\text{m}^{-3}$ , respectively. The GEM concentrations in 2014 were significantly higher than the Northern  
195 Hemisphere back-ground concentration (about  $1.5 \text{ ng m}^{-3}$ ) (Sprovieri et al., 2010) and those  
196 measured in other remote and rural locations in China (Zhang H et al., 2015; Fu et al., 2008a; Fu et  
197 al., 2009). However, in 2016, the GEM concentration ( $1.60 \pm 0.56 \text{ ng m}^{-3}$ ) was similar to the  
198 background concentrations in the Northern Hemisphere. During this period, monthly GEM



199 concentrations showed a significant decrease with a rate of  $-0.60 \text{ ng m}^{-3} \text{ yr}^{-1}$  ( $R^2=0.6389$ ,  $p<0.01$   
200 significance level) (Figure 2).

201 Table 1 showed the Hg variation trends in different regions. Significant decreases of GEM  
202 concentrations in North hemisphere over the past two decades have been well documented (Weigelt  
203 et al., 2015; Cole et al., 2013; Kim et al., 2016). Weigelt et al. (2015) showed that GEM  
204 concentrations decreased from  $1.75 \text{ ng m}^{-3}$  in 1996 to  $1.4 \text{ ng m}^{-3}$  in 2009 at Mace Head, Europe.  
205 Ten-year trends of GEM concentrations at six ground-based sites in the Arctic and Canada also  
206 showed a decreasing trend at a rate of  $13\text{-}35 \text{ pg m}^{-3} \text{ y}^{-1}$  (Cole et al., 2013). In South Korea, the  
207 observed GEM concentration also had significant decrease in recent years (Kim et al., 2016). In  
208 south hemisphere, at the Cape Point of South Africa, GEM concentrations decreased from  $1.35 \text{ ng}$   
209  $\text{m}^{-3}$  in 1996 to  $0.9 \text{ ng m}^{-3}$  in 2008 and rose after then (Martin et al., 2017). However, limited GEM  
210 monitoring sites and relative short-time spans in China restricted the views of long-term trends in  
211 atmospheric Hg concentration in this region. A preliminary assessment indicated that atmospheric  
212 Hg concentrations in China kept increasing before 2012 (Fu et al., 2015). The decreasing trend  
213 observed in our study was accordant with the unpublished data in Mt. Changbai during 2014-2015  
214 cited in the review of Fu et al. (2015). But much sharper decrease of Hg concentrations was observed  
215 in our study. The specific reasons for the Hg concentration decrease in our study will be discussed  
216 in section 3.4. One potential worry is that the calculated trend will be sensitive to seasonal variation  
217 and the missing data in January and February of both 2014 and 2016 may impact the downward  
218 trend. To evaluate the impact of the missing data, we estimate the Hg concentrations in the missing  
219 months based on the least squares method from the data of the same months during 2011-2017  
220 (Figure S1). Combining the estimated data, we re-fit the Hg concentrations and downward trend  
221 still maintained robust and similar to the downward trend in manuscript (Figure 2 and Figure S2).  
222 Thus, we assume that the missing data is not very important and will not impact our main conclusion.

### 223 3.2 Seasonal variation of GEM concentrations

224 Figure 3 showed the monthly variation of GEM concentrations in Chongming Island during the  
225 monitoring period. Observed GEM concentrations showed an obvious seasonal cycle. The mean  
226 GEM concentration in warm season (from April to September) is  $0.29 \text{ ng m}^{-3}$  higher than that in  
227 cold season. Such seasonal variation trend is also observed at Nanjing, Miyun, Mt. Ailao, Mt.



228 Waliguan, and Shangri-La (Zhang et al., 2013; Zhang et al., 2016; Fu et al., 2015; Zhu et al., 2012).  
229 On the other hand, the means of GEM at Mt. Gongga, Mt. Daimai, Mt. Leigong, and Mt. Changbai  
230 in China are relatively higher in cold seasons. The average of atmospheric Hg concentrations in the  
231 north hemisphere also have a trough value in summer (Sprovieri et al., 2016).

232 Seasonal variations of GEM concentration are generally attributed to the following factors,  
233 including natural and anthropogenic emissions, atmospheric chemical reaction, and air mass  
234 transportation. The higher Hg concentrations in cold seasons in Mt. Ailao and Mt. Waliguan were  
235 mainly explained by coal-combustion for urban and residential heating during cold seasons.  
236 Whereas, increasing solar radiation and soil/air temperature dominate the higher Hg concentrations  
237 in Mt. Gongga and Mt. Leigong. In addition, sites in southern, eastern, and northeastern China also  
238 impacted from anthropogenic emissions of GEM from the north and west by the northerly winter  
239 monsoon while the sites located in western, southwestern, and northern China were impacted in  
240 the warm season (Fu et al., 2015). As to most sites in the northern hemisphere, high wet Hg  
241 precipitation induced probably by faster GEM oxidation led to lower Hg concentrations in summer.

242 As to the observation site in Chonming island, we observed almost synchronized trends  
243 between emissions and air Hg concentrations in Figure 4. The annual emissions from both natural  
244 source and anthropogenic source in YRD region (Anhui, Zhejiang, Jiangsu, and Shanghai) was -  
245 0.75 and 10.3 t, respectively. It should be pointed that the natural emissions here is a net natural  
246 emissions, which is the byproducts of a bi-directional Hg flux, time, and area. When the data is  
247 negative, it means GEM dry deposition to the calculated surfaces. Otherwise, it means GEM  
248 emissions to air. The natural emissions varied from -5.4 t to 8.4 t with the highest value in summer  
249 and the lowest value in winter. The anthropogenic emissions were in the range of 2.5-2.7 t, which  
250 is almost unchanged compared to the natural emissions. Therefore, we supposed that the seasonal  
251 cycle of GEM concentrations was dominated by natural emissions (Figure 4). The seasonal trend  
252 of natural emissions is closely related with the canopy types in YRD areas, where widely  
253 subtropical forests, paddy field, and dry farming were observed (Figure S3). The high temperature  
254 will speed up decomposition of organic compound in soil, which lead to Hg emissions from  
255 farmland and forest in YRD region (Luo et al., 2016; Yu et al., 2017). In autumn and winter, with  
256 the decrease of temperature (Table S2), the role of soil changed from Hg source to sink, which



257 reduces the Hg concentrations in the air (Wang et al., 2016). At the same time, the growing  
258 vegetation in autumn also absorbs air Hg, resulting lower Hg concentrations compared to that in  
259 winter. Besides, more air mass transportation from North China and YRD was another reason of  
260 higher Hg concentration in winter than that in autumn. According to the statistics of backward  
261 trajectories in section 3.4, the air mass from North China and YRD region (NW and SW in Table  
262 S3) in autumn and winter accounted for 73% and 95% of the total trajectory in autumn and winter,  
263 respectively. We also noted that the seasonal variation of emissions is more significant than that of  
264 Hg concentrations. Higher wet Hg deposition in summer is a potential impact factor, which reached  
265 about 6.6 times of that in winter (Zhang et al., 2010). On one aspect, abundant Br at the coastal  
266 site of Chongming and higher O<sub>3</sub> concentrations and solar radiation will lead to faster GEM  
267 oxidation in summer.

### 268 3.3 Source apportionment of atmospheric Hg pollutions

269 According to the PSCF result, YRD region, including Shanghai, Jiangsu, Anhui, and Zhejiang  
270 provinces, was the dominant source region in both 2014 and 2016 (Figure 5). Therefore, Hg  
271 emissions from these areas would contribute to high proportion of Hg pollution in Chongming  
272 Island. The offshore area mainly around Jiangsu province also has a high PSCF value because some  
273 trajectories from North China, especially Shandong province, transport to Chongming Island  
274 through this area. Compared to the result in 2014, the PSCF value had an obvious decline in East  
275 China Sea in 2016. This decline may be contributed by the downward trend of GEM concentrations  
276 in north hemisphere (Zhang et al., 2016).

277 PCA method was applied to preliminarily identify the source industries. In the studied period,  
278 totally 2 factors were identified in 2014 and 2016, respectively. The factor 1 had strong factor  
279 loadings of GEM, SO<sub>2</sub>, NO<sub>x</sub>, CO, and PM<sub>2.5</sub> in both 2014 and 2016 (No CO data in 2016 due to  
280 equipment problems). The factor 1 accounted for 49% variance in 2014 and 50% variance in 2016  
281 (Table 2). The results indicated common significant source sectors of the above five air pollutants,  
282 which can also be proven from emission inventories (Table 3). The dominant source industries  
283 included coal-fired power plants, coal-fired industrial boilers, and cement clinker production. The  
284 PCA results showed that anthropogenic emissions were the main sources of GEM during the  
285 sampling period.



286 The factor 2 in 2014 and 2016 both had a strong positive loading on O<sub>3</sub> and negative loading on  
287 NO<sub>x</sub>. The anti-correlation between O<sub>3</sub> and its precursor NO<sub>x</sub> could be an indication of air exchange  
288 between planet boundary layer (PBL) and troposphere. However, the low loading on GEM of factor  
289 2 indicated that Factor 2 had no relationship with GEM concentrations at Chongming from the  
290 aspect of whole year data.

### 291 **3.4 The influence of anthropogenic emissions**

292 To further understand the reason of the downward trend, we firstly compared the meteorological  
293 conditions in both 2014 and 2016. We noted that the difference of annual temperature, solar radiation,  
294 and relative humidity were constrained in the range of  $17.13 \pm 7.48$  °C,  $165.55 \pm 45.87$  W m<sup>-2</sup> and  
295  $75.38 \pm 5.82\%$ , respectively (Table S2). The coefficient of variation for annual mean of these  
296 meteorological conditions in 2014 and 2016 was 2.6%, 6.7% and 0.2%, respectively. In addition,  
297 the wind rose was similar, and the dominating wind was from SE in both 2014 and 2016 (Figure  
298 S4). The HYSPLIT results also provided similar trajectories in 2014 and 2016 (Figure 6). Therefore,  
299 we assumed that the meteorological condition was not the dominant reason of GEM decline at  
300 Chongming site.

301 To further quantify the driver of GEM decline, a trajectory-based analysis method was used in  
302 this study. The 72-h air mass back trajectories were calculated using HYSPLIT for every 8 hours  
303 starting at the observation site. Approximately 918 and 832 trajectories were calculated in sampling  
304 period in 2014 (Mar 1 to Dec 31, 2014) and 2016 (Mar 26 to Dec 31, 2016), respectively. The  
305 trajectories were grouped into 3 clusters in each year according to geographical regions (Figure 6).  
306 The first cluster of trajectories mainly passed through the regions (eg., North China) north and  
307 northwest to Chongming Island before arriving to our monitoring site, which was denoted as cluster  
308 NW. The second cluster mainly passed through the regions west and southwest to Chongming,  
309 which was signed as cluster SW. The third type mainly originated from the East China Seas, South  
310 Korea, Japan and Northeast Asia continent, and then arrived to our monitoring sites directly without  
311 passing the mainland China. This type of trajectories was named as cluster EAST. Some trajectories  
312 originated from the East China Sea and crossed the mainland China before arriving Chongming  
313 were grouped into cluster NW or SW depending on the regions it crossed. The trajectories for each  
314 of the three clusters in 2014 and 2016 were shown in Table 4.



315 Table 4 showed the detail statistics data of the three classifications. From 2014 to 2016, the whole  
316 China region (NW, SW) contributed to 66% of GEM decline at Chongming Island. These results  
317 reflected the effectiveness of existing air pollution control measures in China (SC, 2013; MEP, 2014).  
318 Meanwhile, the NW region, SW region, and EAST region causes 47%, 19%, and 34% for GEM  
319 decline, respectively (Table 4). The largest contribution of reduction was observed in the cluster  
320 NW, suggesting that air pollution controls on anthropogenic emissions in NW region dominated the  
321 recent decrease of GEM concentrations at Chongming site. We also noted that the largest decline of  
322 Hg concentrations was observed in the cluster SW (1.51 ng m<sup>-3</sup>), which indicated more effective air  
323 pollution control in the regions where the air mass of the cluster SW passed. However, since the  
324 proportion of the trajectories in the cluster SW was much less than that in the cluster NW, the  
325 contribution of cluster SW to GEM decline in our observation site was lower.

## 326 4 Conclusion

327 Atmospheric Hg was continuously measured for three years at a regional background site in the  
328 YRD region. During the sampling period, a downward trend for GEM concentrations (-0.60 ng m<sup>-3</sup>  
329 y<sup>-1</sup>) at Chongming Island was observed. The seasonal GEM cycle was dominated by the natural  
330 emissions while the annual GEM concentration trend was mainly impacted by anthropogenic  
331 emissions. By using a new approach that considers both cluster frequency and the Hg concentration  
332 associated with each cluster, we quantified that atmospheric Hg from NW region, SW region, and  
333 EAST region have caused 47%, 19%, and 35% decline of GEM concentrations at Chongming  
334 monitoring site, respectively. The result suggested that reduction of anthropogenic emissions in  
335 mainland China was the main cause of the recent decreasing trend of GEM concentration at  
336 Chongming site. The air pollution control policies in China, especially the pollution control in the  
337 coal-fired power plants, coal-fired industrial boilers, and cement clinker production in YRD region  
338 and Shandong province, have received significant co-benefit of atmospheric mercury emission  
339 reductions. On the other hand, emission reduction from the EAST region, where clusters arrived to  
340 Chongming monitoring site directly without passing the mainland China, implies global effort on  
341 atmospheric Hg emission control under the guidance of *Minamata Convention on Mercury*.  
342 Considering that the *Minamata Convention on Mercury* had come into force in 2017, continuous



343 long-term observation of atmospheric Hg in China will be required for the assessment of policy

344 effectiveness.

345

346 *Data availability.* All data are available from the authors upon request.

347

348 *Competing interests.* The authors declare that they have no conflict of interest.

349

350 *Acknowledge.* This work is sponsored by the Natural Science Foundation of China (No. 21607090),

351 Major State Basic Research Development Program of China (973 Program) (No. 2013CB430000),

352 National Key R&D Program of China (No. 2016YFC0201900)

353

354

355

356

357



## 358 **References**

- 359 Cole, A. S., Steffen, A., Pfaffhuber, K. A., Berg, T., Pilote, M., Poissant, L., Tordon, R., and Hung,  
360 H.: Ten-year trends of atmospheric mercury in the high Arctic compared to Canadian sub-Arctic  
361 and mid-latitude sites, *Atmospheric Chemistry and Physics*, 13, 1535-1545, 2013.
- 362 Draxler, R. R.: Trajectory Optimization for Balloon Flight Planning, *International Journal for*  
363 *Numerical Methods in Fluids*, 5, 13-23, 1996.
- 364 Draxler, R. R., and Hess, G. D.: An overview of the hysplit-4 modeling system for trajectories,  
365 *Australian Meteorological Magazine*, 47, 295-308, 1998.
- 366 Fu, X. W., Feng, X. B., Zhu, W. Z., Wang, S. F.\*, and Lu, J. L.\*: Total gaseous mercury  
367 concentrations in ambient air in the eastern slope of Mt. Gongga, South-Eastern fringe of the Tibetan  
368 plateau, China, *Atmospheric Environment*, 42, 970-979, 2008a.
- 369 Fu, X. W., Feng, X. B., Zhu, W. Z., Zheng, W., Wang, S. F., and Lu, J. Y.: Total particulate and  
370 reactive gaseous mercury in ambient air on the eastern slope of the Mt. Gongga area, China, *Applied*  
371 *Geochemistry*, 23, 408-418, 2008b.
- 372 Fu, X. W., Feng, X. B., Wang, S., Rothenberg, S., Shang, L., Li, Z., and Qiu, G.: Temporal and  
373 spatial distributions of total gaseous mercury concentrations in ambient air in a mountainous area  
374 in southwestern China: implications for industrial and domestic mercury emissions in remote areas  
375 in China, *Science of the Total Environment*, 407, 2306-2314, 2009.
- 376 Fu, X. W., Feng, X. B., Qiu, G. L., Shang, L. H., and Zhang, H.: Speciated atmospheric mercury  
377 and its potential source in Guiyang, China, *Atmospheric Environment*, 45, 4205-4212, 2011.
- 378 Fu, X. W., Zhang, H., Yu, B., Wang, X., Lin, C. J., and Feng, X. B.: Observations of atmospheric  
379 mercury in China: a critical review, *Atmospheric Chemistry and Physics*, 15, 9455-9476, 2015.
- 380 Hong, Q. Q., Xie, Z. Q., Liu, C., Wang, F. Y., Xie, P. H., Kang, H., Xu, J., Wang, J. C., Wu, F. C.,  
381 He, P. Z., Mou, F. S., Fan, S. D., Dong, Y. S., Zhan, H. C., Yu, X. W., Chi, X. Y., and Liu, J. G.:  
382 Speciated atmospheric mercury on haze and non-haze days in an inland city in China, *Atmospheric*  
383 *Chemistry and Physics*, 16, 13807-13821, 2016.
- 384 Hui, M. L., Wu, Q. R., Wang, S. X., Liang, S., Zhang, L., Wang, F. Y., Lenzen, M., Wang, Y. F., Xu,  
385 L. X., Lin, Z. T., Yang, H., Lin, Y., Larssen, T., Xu, M., and Hao, J. M.: Mercury flows in China and



- 386 global drivers, *Environmental Science & Technology*, 51, 222-231, 2017.
- 387 Kim, K. H., Brown, R. J. C., Kwon, E., Kim, I. S., and Sohn, J. R.: Atmospheric mercury at an urban  
388 station in Korea across three decades, *Atmospheric Environment*, 131, 124-132, 2016.
- 389 Landis, M. S., Stevens, R. K., Schaedlich, F., and Prestbo, E. M.: Development and characterization  
390 of an annular denuder methodology for the measurement of divalent inorganic reactive gaseous  
391 mercury in ambient air, *Environmental Science & Technology*, 36, 3000-3009, 2002.
- 392 Lindberg, S., Bullock, R., Ebinghaus, R., Engstrom, D., Feng, X. B., Fitzgerald, W., Pirrone, N.,  
393 Prestbo, E., and Seigneur, C.: A synthesis of progress and uncertainties in attributing the sources of  
394 mercury in deposition, *Ambio*, 36, 19, 2007.
- 395 Luo, Y., Duan, L., Driscoll, C. T., Xu, G., Shao, M., Taylor, M., Wang, S. X, and Hao, J. M.:  
396 Foliage/atmosphere exchange of mercury in a subtropical coniferous forest in south China, *Journal*  
397 *of Geophysical Research Biogeosciences*, 121, 2016.
- 398 Martin, L. G., Labuschagne, C., Brunke, E. G., Weigelt, A., Ebinghaus, R., and Slemr, F.: Trend of  
399 atmospheric mercury concentrations at Cape Point for 1995–2004 and since 2007, *Atmospheric*  
400 *Chemistry and Physics*, 17, 2393-2399, 2017.
- 401 Mason, R. P., Reinfelder, J. R., and Morel, F. M. M.: Bioaccumulation of mercury and  
402 methylmercury, Springer Netherlands, 915-921 pp., 1995.
- 403 Ministry of Environmental Protection (MEP) and State Administration for Quality Supervision and  
404 Inspection and Quarantine (AQSIQ): Emission standard of air pollutants for boilers, MEP, Beijing,  
405 China, 2014.
- 406 Pirrone, N., Keeler, G. J., and Nriagu, J. O.: Regional differences in worldwide emissions of mercury  
407 to the atmosphere, *Atmospheric Environment*, 30, 2981-2987, 1996.
- 408 Polissar, A. V., Hopke, P. K., Paatero, P., Kaufmann, Y. J., Hall, D. K., Bodhaine, B. A., Dutton, E.  
409 G., and Harris, J. M.: The aerosol at Barrow, Alaska: long-term trends and source locations,  
410 *Atmospheric Environment*, 33, 2441-2458, 1999.
- 411 State Council of the People's Republic of China (SC): Action plan of national air pollution  
412 prevention and control, SC, Beijing, China, 2013.
- 413 Schroeder, W. H., and Munthe, J.: Atmospheric mercury—An overview, *Atmospheric Environment*,  
414 32, 809-822, 1998.



415 Sprovieri, F., Pirrone, N., Ebinghaus, R., Kock, H., and Dommergue, A.: A review of worldwide  
416 atmospheric mercury measurements, *Atmospheric Chemistry and Physics*, 10, 8245-8265, 2010.

417 Streets, D. G., Devane, M. K., Lu, Z., Bond, T. C., Sunderland, E. M., and Jacob, D. J.: All-Time  
418 releases of mercury to the atmosphere from human activities, *Environmental Science & Technology*,  
419 45, 10485-10491, 2011.

420 Sprovieri, F., Pirrone, N., Bencardino, M., amp, apos, Amore, F., Carbone, F., Cinnirella, S.,  
421 Mannarino, V., Landis, M., Ebinghaus, R., Weigelt, A., Brunke, E.-G., Labuschagne, C., Martin, L.,  
422 Munthe, J., Wängberg, I., Artaxo, P., Morais, F., Barbosa, H. d. M. J., Brito, J., Cairns, W., Barbante,  
423 C., Diéguez, M. d. C., Garcia, P. E., Dommergue, A., Angot, H., Magand, O., Skov, H., Horvat, M.,  
424 Kotnik, J., Read, K. A., Neves, L. M., Gawlik, B. M., Sena, F., Mashyanov, N., Obolkin, V., Wip,  
425 D., Feng, X. B., Zhang, H., Fu, X., Ramachandran, R., Cossa, D., Knoery, J., Maruszczak, N.,  
426 Nerentorp, M., and Norstrom, C.: Atmospheric mercury concentrations observed at ground-based  
427 monitoring sites globally distributed in the framework of the GMOS network, *Atmospheric  
428 Chemistry and Physics*, 16, 11915-11935, 10.5194/acp-16-11915-2016, 2016.

429 Arctic Monitoring and Assessment Programme and United Nations Environment Programme  
430 (AMAP/UNEP). Global Hg Assessment 2013: Sources, missions, Releases and Environmental  
431 Transport, AMAP/UNEP, Geneva, Switzerland , 2013.

432 Wang, Y. Q., Zhang, X. Y., and Draxler, R. R.: TrajStat: GIS-based software that uses various  
433 trajectory statistical analysis methods to identify potential sources from long-term air pollution  
434 measurement data, Elsevier Science Publishers B. V., 938-939 pp., 2009.

435 Weigelt, A., Ebinghaus, R., Manning, A. J., Derwent, R. G., Simmonds, P. G., Spain, T. G., Jennings,  
436 S. G., and Slemr, F.: Analysis and interpretation of 18 years of mercury observations since 1996 at  
437 Mace Head, Ireland, *Atmospheric Environment*, 100, 85-93, 2015.

438 Wu, Q., Wang, S., Li, G., Liang, S., Lin, C. J., Wang, Y., Cai, S., Liu, K., and Hao, J.: Temporal  
439 Trend and Spatial Distribution of Speciated Atmospheric Mercury Emissions in China During 1978-  
440 2014, *Environmental Science & Technology*, 50, 13428-13435, 2016.

441 Xu, X., and Akhtar, U. S.: Identification of potential regional sources of atmospheric total gaseous  
442 mercury in Windsor, Ontario, Canada using hybrid receptor modeling, *Atmospheric Chemistry and  
443 Physics*, 10, 7073-7083, 2010.



444 Yu, Q., Luo, Y., Wang, S., Wang, Z., Hao, J., and Duan, L.: Gaseous elemental mercury (GEM)  
445 fluxes over canopy of two typical subtropical forests in south China, Atmospheric Chemistry and  
446 Physics Discussions, 1-27, 10.5194/acp-2017-349, 2017.

447 Zhang, G. y., Zhou, L. m., Zheng, X. m., and Huang, W. d.: Temporal Distribution and Potential Hazards  
448 of Wet Deposition Mercury in Yangtze River Estuary, Urban Environmental & Urban Ecology, 1-4, 2010.

449 Zhang, H., Fu, X. W., Lin, C. J., Wang, X., and Feng, X. B.: Observation and analysis of speciated  
450 atmospheric mercury in Shangri-La, Tibetan Plateau, China, Atmospheric Chemistry and Physics,  
451 15, 653-665, 2015.

452 Zhang, H., Fu, X. W., Lin, C.-J., Shang, L. H., Zhang, Y. P., Feng, X. B., and Lin, C.: Monsoon-  
453 facilitated characteristics and transport of atmospheric mercury at a high-altitude background site  
454 in southwestern China, Atmospheric Chemistry and Physics, 16, 13131-13148, 2016.

455 Zhang, L., Wang, S. X., Wang, L., Wu, Y., Duan, L., Wu, Q. R., Wang, F. Y., Yang, M., Yang, H.,  
456 Hao, J. M., and Liu, X.: Updated emission inventories for speciated atmospheric mercury from  
457 anthropogenic sources in China, Environmental Science & Technology, 49, 3185-3194, 2015.

458 Zhang, Y. X., Jacob, D. J., Horowitz, H. M., Chen, L., Amos, H. M., Krabbenhoft, D. P., Slemr, F.,  
459 St Louis, V. L., and Sunderland, E. M.: Observed decrease in atmospheric mercury explained by  
460 global decline in anthropogenic emissions, Proceedings of the National Academy of Sciences of the  
461 United States of America, 113, 526, 2016.

462 Zhao, B., Wang, S. X., Liu, H., Xu, J. Y., Fu, K., Klimont, Z., Hao, J. M., He, K. B., Cofala, J., and  
463 Amann, M.: NO<sub>x</sub> emissions in China: historical trends and future perspectives, Atmospheric  
464 Chemistry and Physics, 13, 9869-9897, 2013.

465 Zhu, J., Wang, T., Talbot, R., Mao, H., Hall, C. B., Yang, X., Fu, C., Zhuang, B., Li, S., Han, Y., and  
466 Huang, X.: Characteristics of atmospheric Total Gaseous Mercury (TGM) observed in urban  
467 Nanjing, China, Atmospheric Chemistry and Physics, 12, 12103-12118, 2012.

468



469 **Figure citation**

470 **Figure 1.** The location of the Chongming monitoring site in Shanghai, China

471 **Figure 2.** Trends of monthly average GEM concentrations and their least squares fit

472 **Figure 3.** Monthly variations of GEM concentration at remote sites in China (Fu et al.,  
473 2015; Sprovieri et al., 2016)

474 **Figure 4.** Seasonal cycle of GEM concentrations and emissions during 2014-2016. The bars  
475 represent the standard deviation of seasonal average.

476 **Figure 5.** Source regions of GEM at monitoring site from PSCF model in 2014(a) and 2016(b)

477 **Figure 6.** The back trajectories map for cluster NW, SW and EAST in 2014(a) and 2016(b)  
478 (NW – Northwest; SW – Southwest; EAST – East).

479



480 **Table citation**

481 **Table 1.** Historical variation trends of atmospheric Hg in previous studies

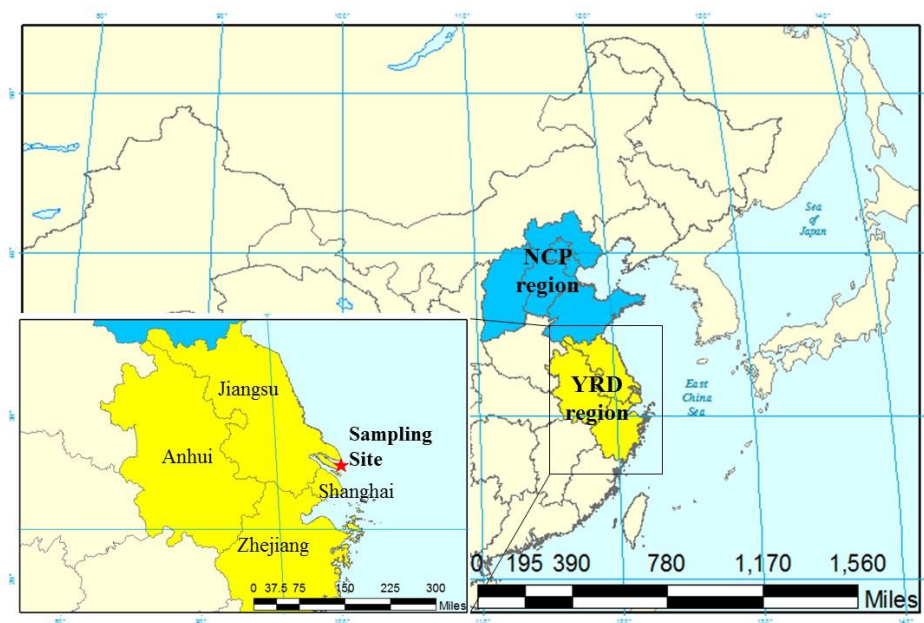
482 **Table 2.** PCA component loading of GEM and the co-pollutants

483 **Table 3.** Main air pollutant emitted by the different sector in YRD region

484 **Table 4.** The statistics of cluster and estimated contribution of GEM reduction in 2014 and 2016

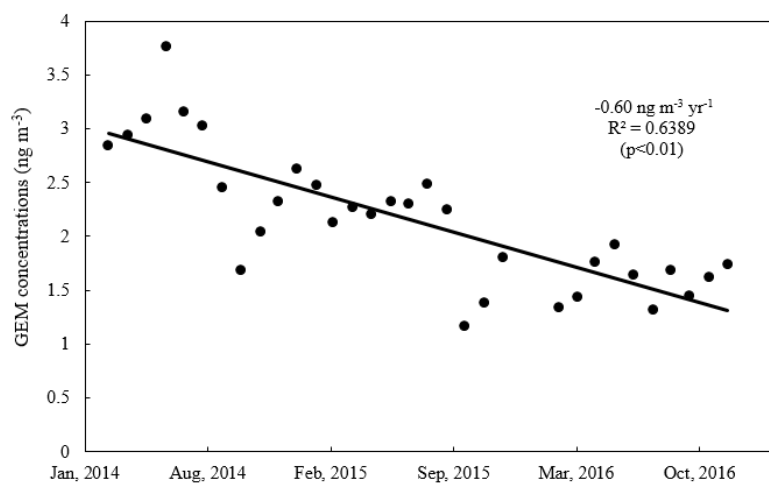
485

486



487 **Figure 1.** The location of the Chongming monitoring site in Shanghai, China

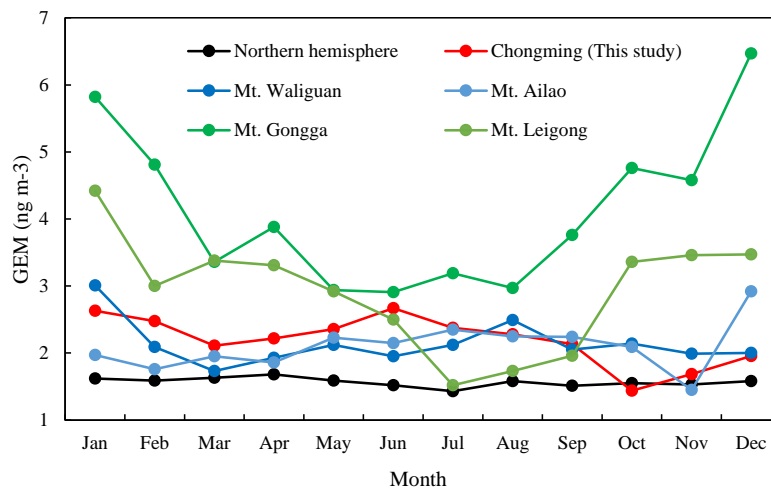
488



489

**Figure 2.** Trends of monthly average GEM concentrations and their least squares fit

490



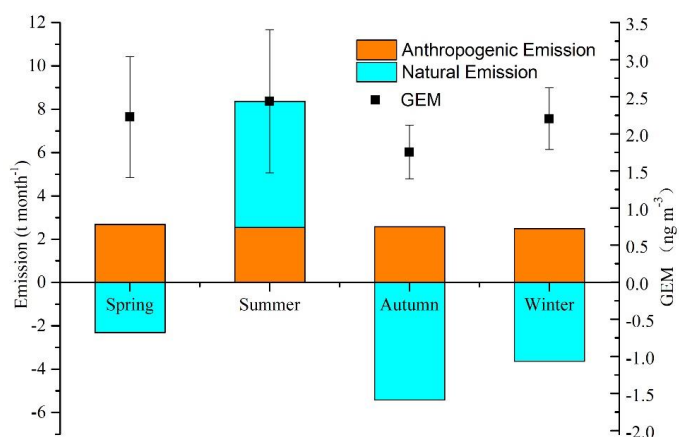
491

**Figure 3.** Monthly variations of GEM concentration at remote sites in China (Fu et al., 2015; Sprovieri et al., 2016)

492

493

494



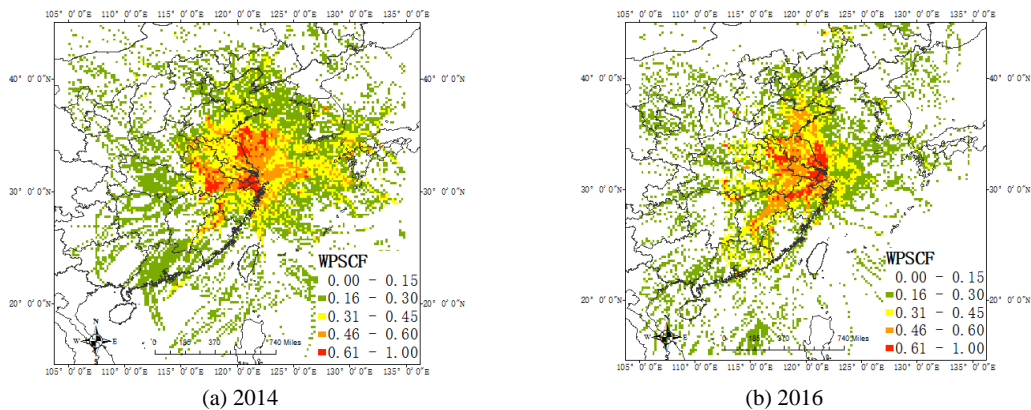
495

496 **Figure 4.** Seasonal cycle of GEM concentrations and emissions during 2014-2016. The bars  
497 represent the standard deviation of seasonal average.

498

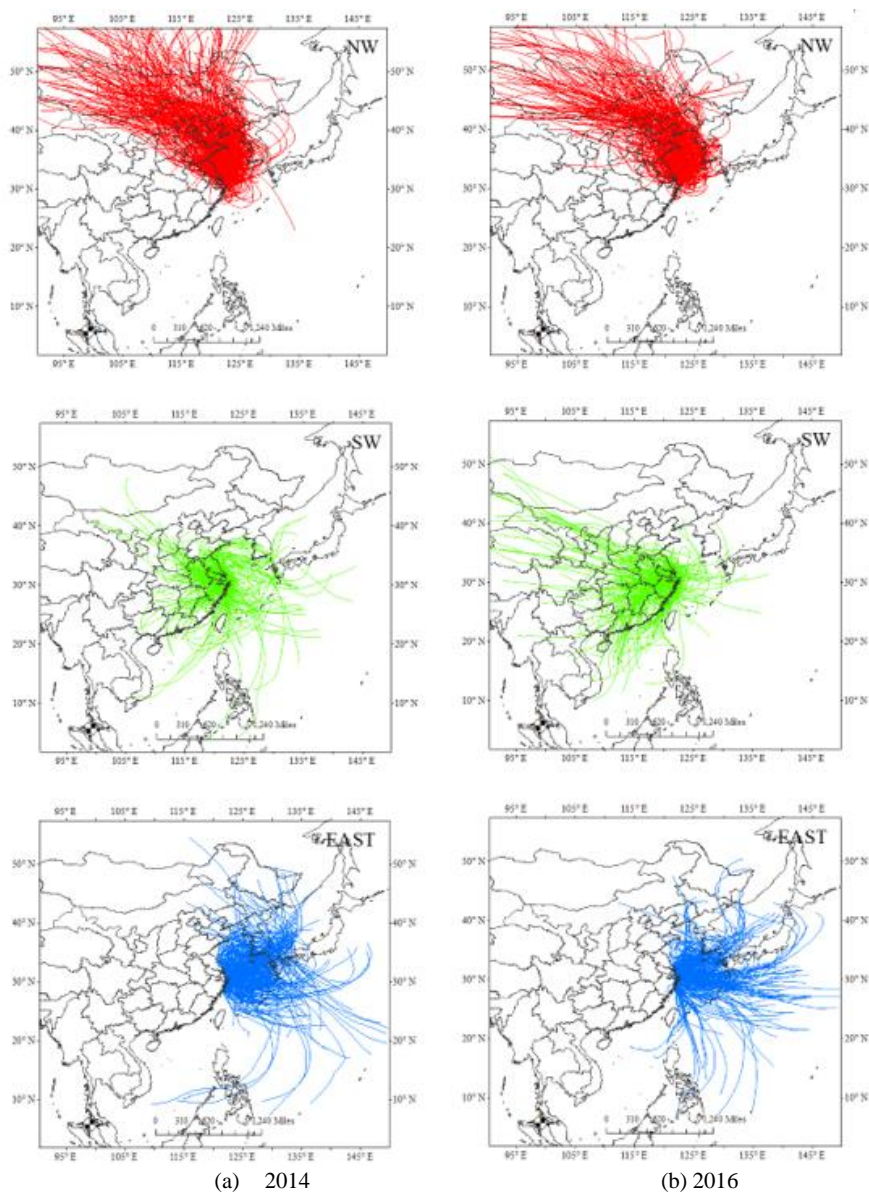


499



500  
501  
502  
503  
504

**Figure 5.** Source regions of GEM at monitoring site from PSCF model in 2014(a) and 2016(b)



505  
506  
507  
508  
509  
510

**Figure 6.** The back trajectories map for cluster NW, SW and EAST in 2014(a) and 2016(b)  
(NW – Northwest; SW – Southwest; EAST – East)



511

**Table 1.** Historical variation trends of atmospheric Hg in previous studies

Monitoring site	Duration	TGM trend (pg m <sup>-3</sup> yr <sup>-1</sup> )	Variation trend	Site description	References
Alert, Canada	2000-2009	-13(-21,0)	-0.9%/y	remote arctic, tundra	Cole et al. 2013
Kuujuarapik, Canada	2000-2009	-33(-50,-18)	-2.1%/y	forest/tundra, sub-arctic	Cole et al. 2013
Egbert, Canada	2000-2009	-35(-44,-27)	-2.2%/y	forest/agricultural, urban within 100km	Cole et al. 2013
Zeppelin Stn, Norway	2000-2009	+2(-7,+12)	no trend	remote arctic mountain ridge, tundra	Cole et al. 2013
St.Anicet, Canada	2000-2009	-29(-31,-27)	-1.9%/y	flat, grassy, rural, urban/industrial within 100 km	Cole et al. 2013
Kejimikujik, Canada	2000-2009	-23(-33,-13)	-1.6%/y	Forested rural	Cole et al. 2013
Head, Ireland	1996-2009		-1.3±0.2%/y	located on the western coast of Ireland, the nearest city is 55km to the east	Weigelt et al. 2015
Hannam dong, South Korea	2004-2011	no trend (3.54±1.46 ng/m <sup>3</sup> )		In the center of Seoul metropolitan city	Kim et al. 2016
Hannam dong, South Korea	2013-2014	decrease to 2.34±0.73 ng/m <sup>3</sup>			Kim et al. 2016
Chongming Island, China	2014-2016	-520	-29.4%/y	remote, wet land and farmland with 20km	This study

512

513

514



515

516

**Table 2.** PCA component loading of GEM and the co-pollutants

	2014		2016		
	Factor 1	Factor 2	Factor 1	Factor 2	
SO <sub>2</sub>	<b>0.763</b>	0.142	SO <sub>2</sub>	<b>0.821</b>	-0.088
NO <sub>x</sub>	<b>0.766</b>	-0.201	NO <sub>x</sub>	<b>0.699</b>	<b>-0.522</b>
O <sub>3</sub>	-0.113	<b>0.977</b>	O <sub>3</sub>	-0.41	<b>0.968</b>
PM <sub>2.5</sub>	<b>0.853</b>	0.052	PM <sub>2.5</sub>	<b>0.875</b>	0.053
GEM	<b>0.664</b>	0.024	GEM	<b>0.775</b>	-0.19
CO	<b>0.793</b>	0.12			
Component	Combustion	Exchange of PBL and troposphere	Component	Combustion	Exchange of PBL and troposphere
Variance explain	49.359	17.525	Variance explain	50.625	75.735

517

518

Note: Text in bold phase were regarded as high loading (factor loading&gt;0.40)



519

**Table 3.** Main air pollutant emitted from the different sectors in YRD region

	SO <sub>2</sub> (kt)	NO <sub>x</sub> (kt)	PM <sub>2.5</sub> (kt)	GEM(t)
Coal-fired power plants	1823.76	1638.31	171.31	18.52
Coal-fired industrial boilers	1526.73	649.94	198.11	17.02
Residential coal combustion	344.57	77.34	95.21	1.04
Cement clinker production	421.17	622.33	362.27	11.56
Iron and steel production	505.03	156.16	240.6	3.99
Biomass incineration	13.99	92.25	556.18	0.61
Other sectors	7225.32	2872.43	832.05	5.39

520

521

522

523

524 **Table 4.** The statistics of cluster and estimated contribution of GEM reduction in 2014 and 2016

Year	Cluster	Trajectories		GEM concentration, $C_j$ ( $\text{ng m}^{-3}$ )	Trajectory weighted concentration, $\text{TWC}_j$ , ( $\text{ng m}^{-3}$ )	Contribution to GEM reduction , $\text{CR}_i$
		Numbers	Ratio			
2014	NW	414	45%	2.46	1.11	
	SW	215	23%	3.37	0.79	
	EAST	289	31%	2.58	0.81	
2016	NW	322	39%	1.56	0.49	47%
	SW	258	31%	1.86	0.62	19%
	EAST	252	30%	1.44	0.35	35%

525

526

527

528

529

530